Observation of demixing in hydrogen-helium mixture at Jupiter's interior conditions.

S. Brygoo[1], P. Loubeyre[1], M. Millot[2], J.R. Rygg[3], P.M. Celliers[2], J. H. Eggert[2], R. Jeanloz[4] and G.W. Collins[3].

[1]Commissariat à l'Énergie Atomique, DAM/DIF, Bruyères-le-Châtel, 91297,Arpajon, France.
[2]Lawrence Livermore National Laboratory, Livermore, California, 94550, USA.
[3]University of Rochester, Department of Mechanical Engineering, Physics and Astronomy, and Laboratory for Laser Energetics, Rochester, New York, 14623, USA.
[4]University of California, Berkeley, California, 94720, USA.

The phase separation in warm dense hydrogen-helium mixtures has been discussed over the past 40 years[1)], with direct consequences for the evolution and interior structure of Jupiter and Saturn. Precipitation of He from the H-He atmosphere at ~ 1-10 Mbar and few thousand Kelvin has been invoked to explain the excess luminosity of Saturn[1)2)] and the depletion of He and Ne observed by the Galileo entry probe of Jupiter's atmosphere[3)4)]. Up to now, only calculations could investigate immiscibility in warm dense H-He mixtures, yet discrepancies remain. Here, we report measurements of the thermodynamic and electronic properties of H-He mixtures under Jovian planetary conditions. These conditions were achieved through laser generated shock waves in H-He samples, pre-compressed in diamond anvil cell targets. A region of immiscibility is observed above 90 GPa at 4.7 kK and below 150 GPa at 10,000 K, coincident with increased electronic conduction. Comparing the present experimental immiscibility domain for the near protosolar H-He mixture to P-T radial profiles for Jupiter suggests H-He phase separation should take place over a significant fraction (about 15% of the radius) of Jupiter's interior. These results give microphysical motivation for recent layered interior models of Jupiter[5)6)] constructed to explain Juno[7)] and Galileo[3)] observations.

Jupiter, Saturn and numerous exoplanets discovered so far, consist mostly of hydrogen and helium[8)]. Evolution and structural models of the Jovian planets are constrained by observational data, e.g. mass-radius relationship, atmosphere composition and inner mass distribution from gravitational moments, and by the microphysics of warm dense hydrogen-helium mixtures. Jupiter is key to understanding the formation, the structure and the evolution of gas giant planets. Exceptional observational data of Jupiter are available thanks to the Galileo[3)] and recent Juno[7)] spacecraft missions. The accepted view now is that Jupiter interior is not isentropic. To match the mass distribution extracted from Juno gravitational moments, it has been proposed that Jupiter's interior is composed of at least four main regions[5)6)]: between the external isentropic homogeneous molecular H_2-He envelope and the second inner isentropic homogeneous metallic H-He envelope, there exits an inhomogeneous non-adiabatic domain likely associated to the demixing of H and He; a fourth region is associated to a slowly eroding core with a compositional gradient of heavier elements. But a puzzling fact is that the H-He phase diagrams suggested recently by the most advanced calculations[9)10)] imply no H-He immiscibility within Jupiter.

Almost 40 years ago, calculations showed there is a close relationship between H-He phase separation and the insulating-to-conducting transition in hydrogen[11]. Yet, the small energy difference between homogeneous and demixed states, as well as the challenges associated with accurate simulating the insulator-conducting transition, makes accurate predictions of the immiscibility region extremely difficult. Recently, significant progress was made by using first principle simulations that go beyond the linear mixing approximation of the two pure species[12]. The temperatures of demixing were first found sufficiently high to cross the Jupiter adiabat[13][14]. However, the demixing domain was inconsistent with low pressure experimental work[15]. Taking into account non-ideal entropy of mixing, the agreement with low pressure demixing data was recovered[9] but the demixing temperatures at high pressure were also lowered significantly with the consequence that the Jupiter's interior profile would not cross the demixing domain. Another calculation[10], performed using the van der Waals exchange and correlation functional, claimed to be better suited to calculate the enthalpy of H-He mixtures[16], and lowered further the demixing temperature to such an extent that the Jupiter isentrope is completely outside the immiscibility region. Collecting experimental data on H-He mixture microphysics under Jupiter's interior condition is needed to assess the uncertainties of calculations.

Here, we report equation of state and electronic properties measurements on a near protosolar H-He mixture at conditions directly relevant for the deep interiors of Jovian planets. Combining static and dynamic compression enables to adjust the temperature versus shock pressure to recreate planetary interior conditions[17][18]. Strong laser shocks from 100 to 300 GPa were used to compress and heat H-He mixtures (11 mol% He in H) that were pre-compressed in a diamond anvil cell to 4 (±0.3) GPa [corresponding to an initial density of 0.278 (±0.007) g/cc]. This technique has previously been applied to measure the properties of warm dense pure helium[19][20] and pure hydrogen[21] but pre-compressions were then limited to 1.6 GPa. DAC modifications have been implemented to be able to reach 4 GPa so that shocks reach temperature-density conditions to address H-He immiscibility under Jovian planetary conditions. The experimental configuration is shown in Fig. 1a. Strong shocks were generated by depositing up to 6 kJ (351 nm light) over 1 ns on the drive surface of the thin front diamond anvil, as delivered by the OMEGA laser at LLE (Laboratory for laser Energetics in Rochester).

The velocity, reflectivity and thermal emission of the shock front propagating in the sample as a function of time were recorded through the back anvil using line-imaging Velocity Interferometer System for Any Reflector (VISAR) and Streaked Optical Pyrometer (SOP) diagnostics. A quartz plate, sitting on the front diamond anvil and pre-compressed with the sample, is used as an in-situ reference for impedance matching, spectral radiance and reflectivity. Typical SOP and VISAR recorded images are shown in figure 1b and 1c. The planarity of the shock wave is very clearly discerned along with the transit time in the quartz and H-He mixture. Pressure, density and internal energy of the H-He shocked state are inferred from the quartz and the H-He mixture shock velocities using the Rankine-Hugoniot conservation relations and impedance matching with quartz as a reference, as previously done for pure He[19][20] and pure H[21]. The optical reflectivity and emission from the shock front during its transit in the quartz are also used to infer the reflectivity and the temperature at the H-He shock front. This analysis framework using quartz as a reference standard has been recently improved[22] and specifically adapted for pre-compressed targets[23]. The lineout of the shock velocity history, superimposed on the raw VISAR image in figure 1c, clearly shows a discontinuity at the quartz-mixture interface and a slightly decaying shock velocity. The reflectance also shows a discontinuity associated with a change of shock front reflectivity between the quartz and the H-He mixture. Out of the 40 shots performed, 26 data points were

entirely successful by showing very good agreement between the two VISAR channels, a good SOP image and a well-positioned time and intensity record for detailing the shock transit through the entire sample. These data for H-He shock pressures ranging from 60 GPa to 280 GPa are presented in the extended data table 1. X additional measurements were also performed along the hugoniot of the 33 mol% He H-He mixture pre-compressed to 2 GPa (data in Extended Data table 2). Both random and systematic uncertainties are included in the reported data points.

Among the measured properties of the shocked H-He mixture along its 4 GPa Hugoniot, the reflectivity is the most clear for detection of demixing. The internal energy, the density, the temperature and the pressure are expected to continuously vary even if demixing is taking place. Upon entering the immiscibility domain, the fraction of the two fluids in equilibrium is continuously evolving and the average density should remain practically constant. Indeed, no sign of phase separation is revealed from the pressure versus compression data (see Extended Data Fig.1). Calculations show a positive excess energy of mixing[12] to be about 10%, and so a phase-separation would thus give rise to a drop of the internal energy. Similarly, the transition to the conducting state, related to the dissociation of the H2 molecule, should be associated to a reduction of the internal energy. These two changes in energy evolution should be entangled, continuous and linearly depending on the concentration changes in the demixed phases or on the fraction of the dissociated molecules. In contrast, a small metal H fraction demixed from the H-He mixture can bring a drastic change of reflectivity. Ab-initio calculations have shown that an increase optical reflectivity at the shock front could be used as a signature of phase separation[25][26][27]. Furthermore, these simulations suggest that the timescale for local phase separation (less than 1 ps) is fast enough to be detected within the experiment time scale (e.g optical skin depth of the shock front divided by the shock wave velocity, calculated larger than 1.3 ps for the shock velocities measured).

Analysis of the VISAR fringes amplitude and intensity at the shock front in H-He using those in quartz as a reference, provides a measurement of the compressed H-He reflectivity. In order to avoid the propagation of systematic uncertainties inherent to this reflectivity analysis, figure 2 presents the raw VISAR fringes data, plotted as the ratio of the weighted average VISAR intensity and amplitude values in the H-He sample over that in quartz, versus the H-He shock velocity. A monotonic behaviour upon increasing shock velocity should be expected when taking the ratio of the reflectivity of any material over the one of quartz in an impedance matching configuration. In contrast here, in Fig. 2, two discontinuities are observed at about 22.1 km/s and 28.4 km/s. These are interpreted as the Hugoniot entering and exiting the H-He immiscibility domain. The sudden increase in sample reflectivity being due to the phase separated fraction of metallic H.

The shock-front reflectivity of the 11mol% He mixture with 4 GPa pre-compression is plotted versus the Hugoniot temperature in Fig. 3. Experimental data are compared to the reflectivity of pure hydrogen under the same pressure-temperature conditions and to the reflectivity of a homogeneous mixture model, as estimated using an interpolation form covering the pure hydrogen reflectivity data set obtained from the many Hugoniot measurements on pre-compressed hydrogen samples from 0.16 GPa to 6 GPa (see Extended Data Fig.2). Ab-initio calculations have shown that the mixing of helium with hydrogen has essentially two effects on the insulator-conducting transition as compared to pure hydrogen: the insulator-conducting transition is shifted to higher pressure-temperature conditions and the reflectivity values of the mixture at saturation are lower than those of pure hydrogen. A simple analytic model was constructed[27] to relate the reflectivity of the H/He homogeneous mixture at a given temperature

and molar density, $\rho_{mixture}$, to the one of pure hydrogen at the effective density, ρ_{Heff} ,with $\frac{1}{\rho_{Heff}} = \frac{1}{x_H}(\frac{1}{\rho_{mixture}} - x_{He}a^3)$ and same temperature (a=1.05 Å, adjusted using ab-initio calculations[27], is very near to the van der Waals radius of the helium atom). This should give an upper bound for the H-He mixture reflectivity since the effect of the He atoms electronic levels mixing with the H electronic density of state are not taken into account by such an effective density scaling. In the inset of Fig. 3, this model operates as expected when compared to reflectivity data taken along the Hugoniot for 33 mol% He mixture pre-compressed to 2 GPa, with good agreement at below 20% reflectivity value and an overestimation above. In contrast, for the 11 mol% He mixture, reflectivity measurements between 4700 K and 10 000 K are situated above the model and match the expected reflectivity of pure hydrogen under the same P-T conditions. About 10 000K, the reflectivity abruptly drops to a saturated value 12 +/- 3% below that of pure hydrogen. The values of the reflectivity at saturation measured on the Hugoniot for the 33 and 11 mol% He pre-compressed mixtures follow the linear concentration dependence expected from simulations (see extended data Fig. 3), however the experimenal change is significantly larger than that obtained in simulations[25][26]. The behaviour of reflectivity versus temperature along the 11 mol% He Hugoniot reveals that hydrogen-helium phase separation occurs between 4,700 K and 10,000K (the location of the discontinuity at 4700 K is deduced from Fig. 2), with reflectivity in this region being consistent with that of pure hydrogen.

In Extended Data Fig. 4, measurements of the energy versus temperature along the 11 mol% He Hugoniot are compared to simulation for a homogeneous protosolar (8 mol% He) mixture. Both are showing a bump over a monotonic sub-linear evolution. The bump in the simulations is ascribed to the H2 molecular dissociation which is interrelated with the insulator-conducting transition[24]. Interestingly, the measured bump is coincident with the first discontinuity in the reflectivity, suggesting that phase separation in the H-He mixture is triggered by the dissociation/ionisation of the H_2 molecules.

The P-T phase diagram of the 11 mol% He mixture is plotted in Fig. 4a. The boundary line of the immiscibility domain is constrained by the two data points determined here from the discontinuity in the reflectivity evolution, respectively at (4,700K, 90 GPa) and at (10,000K, 150 GPa), and by previous low pressure DAC measurements[15]. At low pressure, the immiscibility takes place within the molecular H2-He mixture. The drastic increase of the temperature versus pressure of the immiscibility boundary line in the 100 GPa range is due to the change of nature of the interaction in the hydrogen component from molecular to metallic. There is a large positive energy of mixing between metallic hydrogen and helium that favours phase separation. At pressures higher than 200 GPa, the miscibility gap closure temperature is predicted to remain nearly constant with pressure, at least until helium ionizes. Calculations[28] that best match He ionization data at few hundred GPa conditions[20] suggest He ionization may not occur in Jupiter's interior (see extended data Fig. 5). In Fig. 4b, various profiles of Jupiter's interior are plotted in the phase diagram of the protosolar H-He mixture (the change of concentration from 11 to 8 mol% He results in a slight decrease of the temperature, about 600 K at 200 GPa, as estimated using ab-initio calculations[13][14]). Jupiter's isentropes, calculated using various ab-initio H-He equations of states[29] and the non-isentropic Jupiter profile[6], recently constructed to match the Juno and Galileo constraints, all cross the immiscibility domain. The experimental immiscibility domain extends to significantly higher temperature than predicted by the most advanced ab-initio calculations[9][10].

We show here that, even taking into account the uncertainty for the Jupiter's interior profile, hydrogen-helium demixing likely exists inside Jupiter. As shown in figure 4c, the H-He phase separation could take place over a significant fraction of Jupiter's interior, about 15 % of the radius, an estimation made assuming a constant helium distribution throughout the interior. That demixed layer is in good agreement with the inhomogeneous domain which had to be constructed in an advanced model[6] to reproduce Juno and Galileo spacecrafts observations. Finally, the role of H-He demixing had been invoked long ago to explain the high luminosity of Saturn[1,2]. Recent modelling of the cooling behaviour of Saturn[30] indicates that the H-He immiscibility domain should extend to higher temperature compared to ab-initio calculations, and that is confirmed by the present data.

References.

1) Salpeter, E. On convection and gravitational layering in Jupiter and in stars of low mass. Astrophys . J. 181, L83-L89 (1973).
2) Fortney, JJ and Hubbard, WB. Phase separation in giant planets: inhomogeneous evolution of Saturn. Icarus 64, 228 -243 (2003).
3) Von Zahn, U. & Hunten, D.M. The helium mass fraction in Jupiter's atmosphere. Science 272, 849 – 851 (1996).
4) Wilson, H.F. & Militzer, B. Sequestration of noble gases in giant planet interiors. Phys. Rev. Lett. 104, 121101 1-4 (2010).
5) Wahl, S.M. et al. Comparing Jupiter interior structure models to Juno gravity measurements and the role of a dilute core. Geophys. Res. Lett. 44, 4649 -4659 (2017).
6) Debras, F. and Chabrier, G. New models of Jupiter in the context of Juno and Galileo. The Astrophys. J. 872, 100 (12 pp) (2019).
7) Bolton, S.J. et al. Jupiter's interior and deep atmosphere: the initial pole-to-pole passes with the Juno spacecraft. Science 356, 321 – 825 (2017).
8) Guillot, T. & Gautier, D. Giant planets, volume 10 of Treatise on Geophysics 2nd edition, (Shubert G. and Spohn T. Eds, Elsevier (2014)).
9) Morales, M., Hamel, S., Casperson, K. & Schwegler, E. Hydrogen-helium demixing from first principles: from diamond anvil cells to planetary interiors. Phys. Rev. B 87, 174105 1-4 (2013).
10) Schotler, M. and Redmer, R. Phys. Rev. Lett. 120, 115703 (2018).
11) Stevenson, D.J. & Salpeter, E.E. The phase diagram and transport properties for hydrogen-helium fluid planets. The Astrophysical J Suppl. Series 35, 221-237 (1977).
12) Vorberger, J., Tamblyn, I., Militzer, B. & Bonev , S.A. Hydrogen-helium mixtures in the interiors of giant planets. Phys. Rev. B 75, 024206 1-11 (2007).
13) Lorenzen, W., Holst, B. & Redmer, R. Demixing of hydrogen and helium at Megabar Pressures. . Phys. Rev. Lett 102, 115701 (1-4) (2009).
14) Morales, M.A., Schwegler, E., Ceperley, D., Pierleoni, C., Hamel, S. & Casperon, K. Phase separation in hydrogen-helium mixtures at Mbar pressures. PNAS 106, 1324 -1329 (2009).
15) Loubeyre, P., LeToullec, R. & Pinceaux, J.P. Binary phase diagrams of H2-He mixtures at high temperature and high pressure. Phys. Rev. B 36, 3723 - 3730 (1987).
16) Clay III, R.C, Holzmann, M., Ceperley, D. and Morales, M. Benchmarking density functionals for hydrogen-helium mixtures with quantum Monte Carlo: Energetics, pressures and forces. Physical Review B 93, 035121 (2016).
17) Loubeyre, P. et al. Coupling static and dynamic compressions: first measurements in dense hydrogen. High Press. Res. 24, 25-31 (2004).
18) Jeanloz, R. et al. Achieving high-density states through shock-wave loading of precompressed samples. PNAS 104, 9172-9177 (2007).
19) Eggert, J. et al . Hugoniot of helium in the ionization regime. Phys. Rev. Lett. 100, 124503 (2008).
20) Celliers, P. et al. Insulator-to-conducting transition in dense fluid helium. Phys. Rev. Lett. 104, 184503 1-4 (2010).

21) Loubeyre, P. et al. Extended data set for the equation of state of warm dense hydrogen isotopes. Phys. Rev. B 86, 144115 1-9 (2012).
22) Knudson, M. & Desjarlais, M.P. Adiabatic release measurements in α-quartz between 300 and 1200 GPa: Characterization of α-quartz as a shock standard in the multimegabar regime. Phys. Rev. B 88, 184107 1-18 (2013).
23) Brygoo et al. Analysis of laser shock experiments on precompressed samples using a quartz reference and application to warm dense hydrogen and helium. Journal of Applied Physics, 118, 195901 (2015).
24) Militzer, B. & Hubbard, W.B. Ab initio equation of state for hydrogen-helium mixtures with recalibration of the giant-planet mass-radius relation. The Astrophysical J 774, 148 1-11 (2013).
25) Hamel, S., Morales, M.A. & Schwegler, E. Signature of helium segregation in hydrogen-helium mixtures. Phys. Rev. B 84, 165110 1-7 (2011).
26) Soubiran, F. , Mazevet, S., Winisdoerffer, C. & Chabrier, G. Optical signature of hydrogen –helium demixing at extreme density-temperature conditions. Phys. Rev. B 87, 165114 1-5 (2013).
27) Soubiran, F. PhD thesis. Ecole Normale Supérieure de Lyon, pp 91-94 (2012).
28) Soubiran, F.K, Mazevet, S., Winisdoerffer, C. and Chabrier, G. Helium gap in the warm dense matter regime and experimental reflectivity measurements. Phys. Rev. B 86, 115102 (1-3) (2012).
29) Millitzer, B., Soubiran, F., Wahl, S.M. and Hubbard, W. Understanding Jupiter's interior. J. Geophys. Res. Planets 121, 1552 – 1572 (2016).
30) Püstow, R., Nettelmann, N., Lorenzen, W. and Redmer, R. H/He demixing and the cooling behavior of Saturn. Icarus 267, 323 -333 (2015).

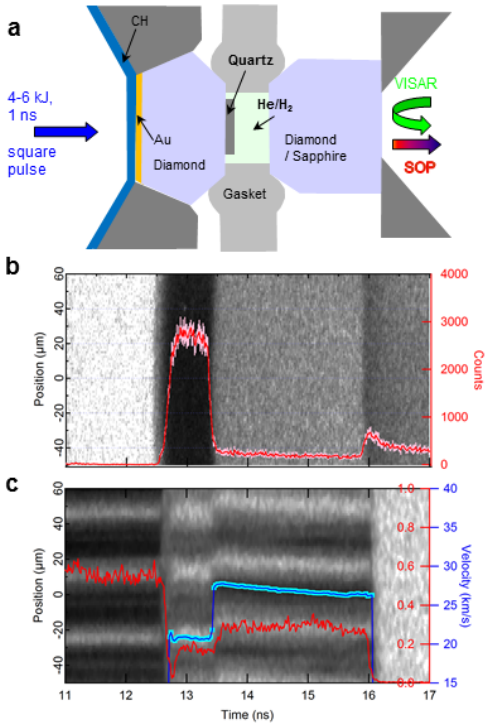

Figure 1: Experimental configuration for laser shocks in the pre-compressed target and representative line-imaging pyrometer (SOP) and interferometric Doppler velocimeter (VISAR) data. (a) Sketch of the target assembly. The laser, by ablating the CH layer, generates a shock that propagates from left to right into the first diamond anvil (~360 μm thick) then the quartz plate (~15 μm thick) before entering the 4 GPa pre-compressed H-He mixture (~40 μm thick). A gold layer between the plastic ablator and the diamond anvil is used to screen ~keV x-ray radiation produced at the ablation surface from pre-heating the sample. 4 GPa pre-compression was achieved by using conical window inserted in the tungsten-carbide support instead of the flat support geometry[19)20)21)]. Because the optical transmission of the diamond window showed a perturbed transmission at high laser intensity, sapphire anvil were also used. Optical SOP and VISAR measurements are

performed through the back anvil. (b) SOP and (c) VISAR images obtained for shot 85578 which a sapphire anvil. (c) Shock front velocity history (blue line) is extracted from the VISAR image with an accuracy of ~1-2 %. The normalized fringe intensity of the VISAR signal (red line) is used to determine reflectivity

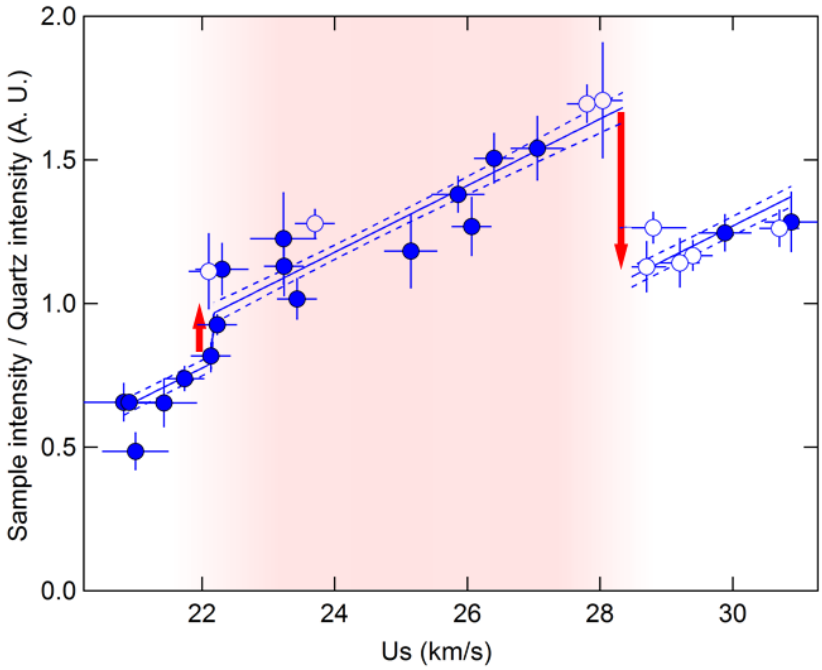

Figure 2: Ratio of the VISAR output at the shock front in the H-He mixture over that in quartz versus shock velocity in the H-He mixture. This output is a weighted average between the amplitude of the fringes using a Fourier analysis and the average intensity over several fringes (see method). Errors bars show 1-σ random uncertainties. Experiments with both diamond (filled circles) and sapphire (open circles) anvils are included. Discontinuous jumps in the intensity ratio are observed at 22.1±0.3 km/s and 28.5±0.5 km/s, indicated by the red arrows. Quartz is known to have a smooth VISAR intensity in this velocity range. Also shown are a piecewise linear fit (solid line) with uncertainties (dotted lines), as well as the domain where H-He phase separate along the Hugoniot (shaded pink) as in all figures throughout the paper.

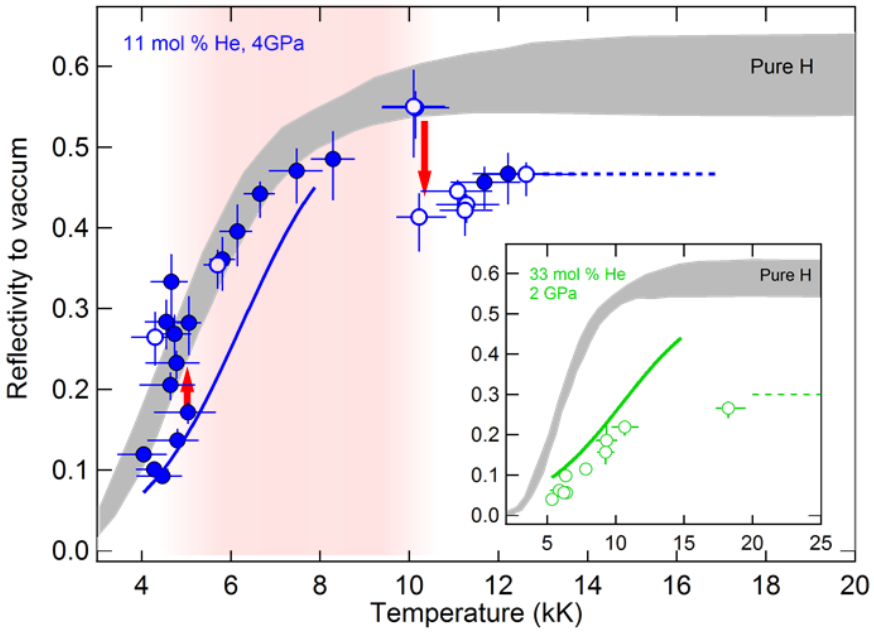

Figure 3: Reflectivity vs Temperature along the Hugoniot for H-He mixtures with 11 (blue) and the 33 (inset green) mol% He. Filled and open circles indicate data collected through the diamond and sapphire anvils respectively. Errors bars include random and systematic uncertainties. The grey curve is the reflectivity of pure hydrogen estimated along the P-T conditions of the H-He Hugoniot using the fit given in Extended Data Fig. 2; its thickness represents standard deviations at the 1σ level. The solid line is Soubiran's ab-initio based scaling model that relates the reflectivity of a homogeneous H-He mixture to that of pure hydrogen[27]: it should reproduce well the onset of reflectivity and should be an upper bound towards saturation as observed for the 33 mol% mixture. In contrast, for the 11 mol% data points lie above the model with values of reflectivity similar to pure hydrogen indicating demixing. The dashed-lines indicate the experimental saturation of reflectivity on the Hugoniot. The two red arrows correspond to the two discontinuities observed in Fig. 2 and indicate reflectivity changes when the 11 mol% He mixture enters and exits the demixing region.

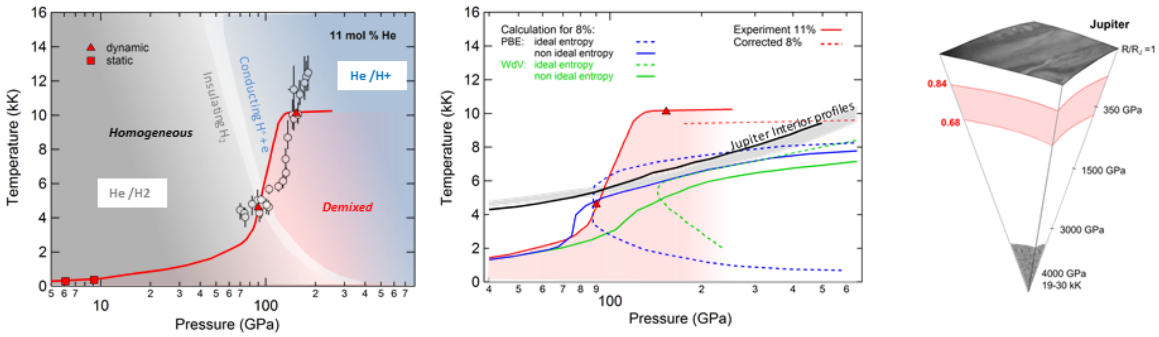

Figure 4: Phase diagram of the near protosolar hydrogen-helium mixture and Jupiter's interior implication. (a) Phase diagram measured for the 11 mol% He mixture: the two red triangles and the two red squares are the data on the immiscibility domain measured here by dynamic compression and previously by static compression [15]. The red line interpolates between these points, using the H2-He demixing calculated slopes from ref. 31 up to 60 GPa and the H-He demixing calculated horizontal slope from ref.9&10 above 200 GPa. The phase diagram is split in two ways: first, based on the miscibility of hydrogen and helium (above red line: homogenous and below: demixed), and second, based on the conductivity of the hydrogen component (grey: molecular and blue: dissociated and ionized).The white boundary between the insulating and conducting regions is determined based on previous measurements by laser shocks in pre-compressed targets (ref. 31 and Extended Data Fig. 2) and by multi-shocks compression on cryogenic-targets[32) 33)] below 2kK. The circles are the present Hugoniot measurements. (b) Comparison between the experimental and calculated immiscibility domain for the near protosolar (11 mol% He) H-He mixture. Red curve is experiment; the red dashed line is the corrected boundary for the protosolar (8 mol% He) composition. The blue and green curves show DFT calculations under various approximations: blue and green indicating the use of PBE[9)] and VdW functionals[10)] respectively; The dashed lines are for ideal mixing and full lines for explicit entropy calculation. The black line is the non-isentropic Jupiter's profile of ref.6 and the thick grey curve the envelope of three Jupiter's isentropes based on different hydrogen-helium equation of state[24)34)35)]. (c) The H-He phase separated layer inside Jupiter as inferred from panel (b).

Methods.

Properties of the H2-He mixtures in the pre-compression state.

The Hugoniot curve for two mixtures was studied. One composed of helium (20 mol % He) and molecular hydrogen (80 mol % H_2) at an initial pressure of 4 GPa; the other composed of helium (50 mol % He) and molecular hydrogen (50 mol % H_2) at an initial pressure of 2 GPa. The initial pressure in the pre-compressed target was measured just before each shot using the ruby luminescence pressure scale[36]. The density and the refractive index in this un-shocked initial state are estimated using ideal mixing rules from measurements in pure helium[37] and in pure hydrogen[38]. The density is thus given by:

$$\rho\left(\frac{g}{cm^3}\right) = \frac{4x_{He} + 2.02x_{H2}}{v_{He}x_{He} + v_{H2}x_{H2}}$$

where xHe and xH2 are the molar fractions of He and H_2, respectively.The experimental specific volumes for He and H_2 are given by:

$$v_{He}\left(\frac{cm^3}{mol}\right) = 23.810{P_0}^{-1/3} - 17.833{P_0}^{-2/3} + 29.760{P_0}^{-1}$$

$$v_{H2}\left(\frac{cm^3}{mol}\right) = 36.40083{P_0}^{-1/3} - 23.5919{P_0}^{-\frac{2}{3}} + 27.9069{P_0}^{-1}$$

with P_0 in kbar.

Within the framework of the Lorenz-Lorentz relation which relates the refractive index of a medium to its atomic polarizability, the most frequently used mixing rule is a linear combination of the Lorenz-Lorentz factor, $F_{ll,}$ of the different components of the mixture, giving here:

$$\frac{1}{\rho}\frac{n^2 - 1}{n^2 + 2} = x_{He}F_{ll\,He} + x_{H2}F_{ll\,H2}$$

$F_{ll\,He}$, $F_{ll\,H2}$, ρ_{He} and ρ_{H2} are determined at the initial pressure P_0 , as reported in Dewaele et al.[39].

A 20 (50) mol/% He-H2 mixture is equivalent to a 11(33) mol/% He-H mixture. This latest notation is used throughout the main paper because most of the reported data are in a regime where H2 molecules are dissociated and also, the He-H concentration is generally specified for astrophysical applications.

Experimental configuration and diagnostics (VISAR and SOP).

Samples were shock compressed by direct-drive laser ablation at the Omega Laser Facility, Laboratory for Laser Energetics (LLE) of the University of Rochester, NY (USA) using 1-6 kJ of 351 nm UV laser in a 1 ns flat-top temporally shaped pulse; distributed phase plates create a super-Gaussian spatial distribution matching the surface (1.1 mm in diameter) of the diamond window accessible through the diamond anvil cell optical aperture.

Our primary diagnostics were the Velocity Interferometer System for Any Reflector (VISAR) and the Streaked Optical Pyrometer (SOP). The VISAR offers a line-imaging, time-resolved record of the velocity of moving reflecting interfaces and optical properties (reflectivity, absorption) at the probe laser wavelength, 532 nm. The fringe phase encodes the apparent velocity history while the fringe amplitude records the reflectivity of the tracked moving interface and the absorption of the medium through which the probe laser is passing[40]. Two different sets of sensitivities were used for all the experiments, as given by the couple of values for the velocity per fringe in vacuum set respectively for each of the two interferometers: either (2.73 km/s and 6.91 km/s) or (16.08 km/s and 6.91 km/s).To obtain the true velocity, one has to divide the apparent velocity by the refractive index of the H-He mixture at the pre-compression pressure.

In addition to velocity, the reflectivity of the target can be extracted from the intensity of the VISAR fringes. Two different methods can be used. The first one is the Fourier analysis done to extract the phase (velocity) which gives also the fringe amplitude, directly proportional to the reflectivity of the target. The second one consists on taking an intensity profile of the target (average over several fringes) over time. The contrast of the fringes is therefore averaged over the overall intensity. The background needs to be considered carefully because it can offset the signal and bias the ratio toward 1. Ghost fringes from non-moving surfaces have different consequences in both methods: decreasing the contrast with the Fourier analysis and increasing the background when extracting the profile. For each VISAR channel, both methods have been applied and are generally in good agreement. The ratio of the sample signal to the quartz signal and its uncertainty is taken as the weighted average of both methods on both channels.

The SOP acquires a line-imaging time-resolved measurement of the spectral radiance of the shocked sample integrated over the domain 590 nm - 850 nm[41]. The temperature can then be deduced from this measured thermal emission, under the assumption of a grey-body spectral radiance at an effective wavelength λ_0 = 650 nm, giving:

$$I = \frac{A\varepsilon(\lambda_0)}{e^{hc/\lambda_0 kT} - 1}$$

where $\varepsilon(\lambda_0)$is the emissivity given by (1-R), with R the measured optical reflectivity, A is a constant that incorporates the transfer factor of the optical system and the response of the detector. Inverting this expression to solve for temperature gives:

$$T = T_0 \frac{1}{\ln\left(\frac{\varepsilon(\lambda_0)A}{I} + 1\right)}$$

where $T_0 = hc/\lambda_0 kT$ is related to the effective wavelength of the passband of the pyrometer (T0 = 1.9 eV at λ_0 = 650 nm). Since the temperature determination is made relative to the quartz reference, the temperature in the sample is determined from the ratio of the signal levels observed in the quartz and in the sample, such that the system calibration constant A drops out of the expression and so:

$$T_S = T_0 \frac{1}{\ln\left(e^{\frac{T_0}{T_Q}} - 1\right)\frac{I_Q^*}{I_S^*} + 1}$$

with $I^* = I_{ADU}/(1-R)$, I_{ADU} being the analog-to-digital counts associated with the observed signal, and R being the reflectivity measured with the VISAR. Knowing the shock velocity in quartz, the temperature in quartz, T_Q, is estimated from the published calibrated function $T_Q(Us)$[23]. This expression is true as long as the calibration constant A is the same for the quartz and for the sample. Upon using diamond optical anvils, because of possible modification of the transmission of the window due to x-ray blanking, measurements were made over 200 ps on each side of the quartz/H-He mixture shock breakout so that A has no time to change significantly.

Reflectivity of pure hydrogen.

The reflectivity of pure hydrogen, at the P-T conditions of the H-He Hugoniot curves experimentally covered in the present study, has been estimated by directly interpolating between experimental data on pure hydrogen, using a fit that reproduces various Hugoniot curves of pre-compressed hydrogen, already published[21)23)] for pre-compression from 0.16 GPa to 1.6 GPa and recently measured for pre-compression in between 5.4 GPa and 6 GPa (see Extended Data table 3). The fitting form chosen here to reproduce these reflectivity data is similar to the one used to described the dissociation fraction of the H2 molecule in the hydrogen ab-initio based EoS[42)]. The fit, as shown in Extended Data Fig.2, has been obtained using the orthogonal distance regression approach taking into account error bars in density (g/cm3), reflectivity and temperature (kK). It is given by:

$$R = \frac{0.55}{e^{\frac{8.77}{T} - 8.08\,T\rho^{2.74}} + 1}$$

To estimate the reflectivity along a particular Hugoniot and the uncertainty associated to it, a Monte Carlo approach has been used. Thousand data sets have been randomly generated within the uncertainties in density, temperature and reflectivity. and for each obtained fit, the reflectivity along the desired Hugoniot is estimated. The thick gray line in figure 3 (and its

inset) represents the 1σ standard deviation envelope of the H reflectivity along the P-T path associated to the H-He mixture Hugoniot.

Estimation of error bars .

There are two types of errors that have to be taken into account and propagated: random errors coming from uncertainty in observables (shock velocities, index of refraction, initial density of the sample and of the quartz reference, counts for reflectivity and temperature estimates) and systematic errors coming from uncertainty in the EOS of the standard used (precision of the different fits used: principal Hugoniot, precision of the model used to take into account the precompression[23]). These two types of errors are independent and can therefore be treated separately.

Random errors in pressure and density: these errors are essentially calculated by propagating the uncertainty in the measurements of the two observables, i.e Us_{quartz} and Us_{sample}, within the impedance-matching construction and in the initial density, coming from the initial ruby pressure uncertainty. The error in the quartz velocity implies that there is a set of possible release states and therefore a set of possible final states for the sample. The number of sample states is further increased by the error in the shock velocity of the sample. Uncertainties are propagated using a Monte-Carlo routine. A set of several thousand final points is generated from a combination of possible initial states and possible velocities determined by the uncertainties measurements. A histogram of the result is then generated and the positive and negatives errors are obtained by calculating the standard deviation around the nominal value.

Random errors in reflectivity and temperature: Uncertainties in reflectivity and temperatures are also calculated using a Monte-Carlo routine to propagate errors in the intensity of the VISAR measurements and of the SOP measurements.

Systematic uncertainties: In the reference quartz model used here[23], the errors are stemming from the uncertainty in the quartz principal Hugoniot fits (Us vs Up and T vs Us) and from the release model for shocked quartz. Again these types of error are independent and can therefore be easily propagated.

Change of diamond anvil optical transmission due to blanking under x-ray loading.

The transparency of the diamond window in the visible can be strongly altered by absorbing the x-ray radiation emitted within the plasma plume generated by the ablation of the plastic layer at irradiance in the vicinity of 10^{15} W/cm^2. This photoionization induces a transient partial opacity of the diamond anvil. That is illustrated in Extended data Fig.6. In most cases, the transmission through a photo-ionized diamond window recovers and can be modeled[43] as $(1-\exp(-t/\tau))$ with τ in the ns range. The SOP signal and the reflected VISAR laser intensity, measured at the shock front, are thus a convolution of the intrinsic time dependence signal from the shock front and of the optical transmission of the diamond anvil. However, since reflectivity

and temperature measurements are made relative to quartz, the perturbation due to the change of the diamond transmission can be minimized by making relative measurements on each side of the breakout from quartz to H-He sample over a small enough (100-200 ps) time scale so that the optical transmission of the diamond anvil can be considered invariant. Uncertainties arising from this effect are included in the error bars.

Some experiments were also performed with a sapphire anvil window (though much more difficult to operate than diamond for a 4 GPa pre-compression). Sapphire is less susceptible to the transient opacity from the x-ray loading than diamond. Data obtained using diamond or sapphire anvil windows are in good agreement.

References.

31) Schouten, J.A., de Kuijper, A. and Michels, J.P. Critical ,line of He-H2 up to 2500 K and the influence of attraction on fluid-fluid separation. Phys. Rev. B 44, 6630 – 6634 (1991).
32) Knudson, M.D. et al. Direct observation of an abrupt insulator-to-metal transition in dense liquid deuterium. Science 348, 1455 – 1460 (2015).
33) Celliers, P.M. et al. Insulator-metal transition in dense fluid deuterium. Science 361, 677 – 682 (2018).
34) Nettelman, N., Becker, A., Holst, B. and Redmer, R. Jupiter models with improved ab-initio hydrogen equation of state (H-REOS.2). Astrophys. J. 750, 52 (2012).
35) Saumon, D., Chabrier, G. and Van Horn, H.M. An equation of state for low-mass stars and giant planets, Astrophys. J. 99, 713 (1995).
36) Mao, H.K. , Xu, J. and Bell, P.M. Calibration of the ruby gauge to 800 Kbar under quasi-hydrostatic conditions. J. Geophys. Res. : Solid Earth 91, 4673-4676 (1986).
37) Le Toullec, R., Loubeyre, P. a,d Pinceaux, J.P. Refractive-index measurements of dense helium up to 16 GPa at T=298 K: Analysis of its thermodynamic and electronic properties. Phys. Rev. B 40, 2368-2378 (1989).
38) Mills R. L., Liebenberg, D.H. and Bronson, J.C. Equation of state of fluid n-D2 from P-V-T and ultrasonic velocity measurements. J. Chem Phys. 68, 2663-2668 (1978).
39) Dewaele A., Eggert, J., Loubeyre, P. and LeToullec, R. Measurement of refractive index and equation of state in dense He, H2, H2O, and Ne under high pressure in a diamond anvil cell. Phys. Rev. B 67, 094112 1-8 (2003)
40) Celliers P. M. et al. Line-imaging velocimeter for shock diagnostics at the OMEGA laser facility. Rev. Sci. Instrum. 75, 4916 - 4920 (2004).
41)) Miller J. E. et al. Streaked optical pyrometer system for laser-driven shock-wave experiments on OMEGA. Rev. Sci. Instrum. 78, 034903 1-7 (2007).
42) Caillabet L., Mazevet, S. and Loubeyre, P. Multiphase equation of state of hydrogen from ab-initio calculations in the range 0.2 to 5 g/cc up to 10 eV. Phys. Rev. B 83, 094101 1-15 (2011).
43) Eggert J. et al. Melting temperature of diamond at ultra-high pressure. Nat. Phys. 6, 40-43 (2010).

Acknowledgements We gratefully acknowledge M. Millerioux and F. Occelli for help in the preparation of the pre-compressed targets. We thank F. Soubiran and S. Hamel for useful discussions and F. Soubiran for sharing unpublished data. We thank the OMEGA laser facility management, staff and support crew for excellent shots and diagnostic support with special thanks to C. Sorce, A. Sorce and J. Kendrick. The OMEGA Laser Facility shots were allocated under the NLUF programme. Part of this work was prepared by LLNL under contract number DE-AC52-07NA27344 with support from LLNL LDRD program and the US Department of Energy

Fusion Energy Sciences Program. This work was performed under the auspices of a cooperation agreement CEA/DAM and DOE/NNSA on fundamental sciences. Partial funding for G.W.C. and J.R.R. was provided by NSF Physics Frontier Center award PHY-2020249 and DOE NNSA award DE6NA 0003856.

Extended DATA

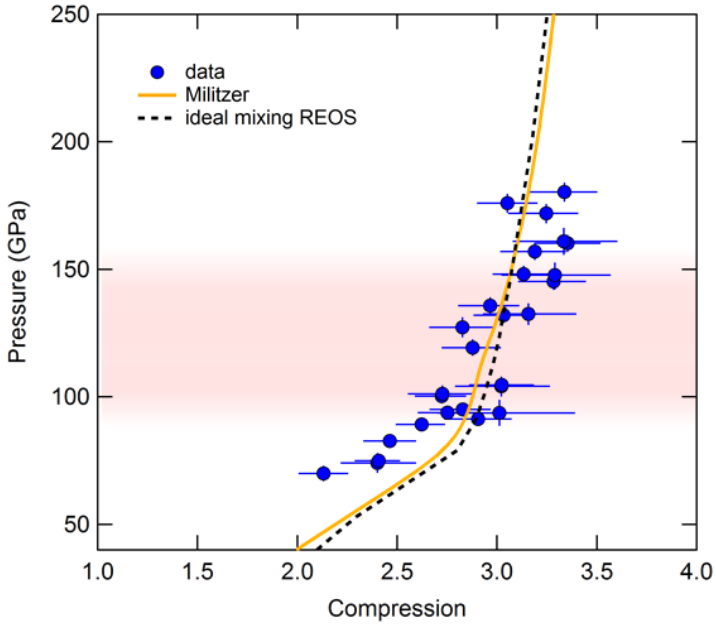

Extented Data Fig. 1: Compression curve of the Hugoniot for the 11 mol% He H-He mixture. Full dots indicate experimental data for the mixture pre-compressed to 4 GPa (average initial density of 0.2766 g/cm^3). Error bars include random and systematic uncertainties. The full yellow and the dashed black lines are respectively simulations for a 8 mol% He mixture[24)] and a REOS linear mixing calculation of the equation of state for the 11 mol% He mixture [34)].

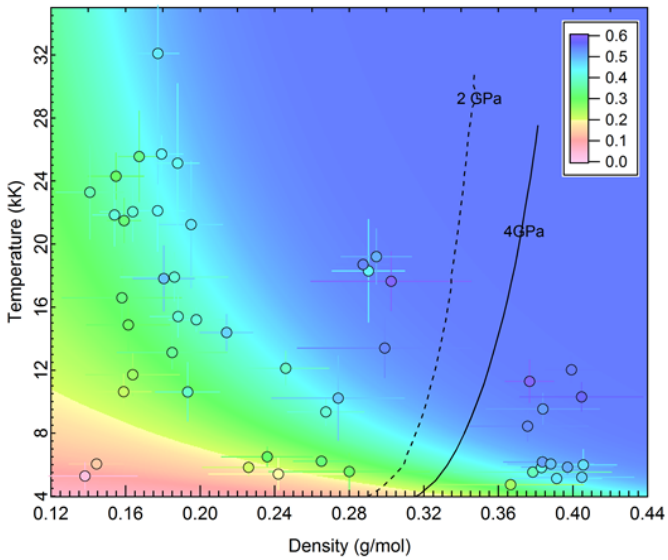

Extended Data Fig.2: Reflectivity of pure hydrogen versus temperature and density. Circles are the experimental data points, published below 0.32 g/mole (see ref. 23) and unpublished above (see Extended data table 3). The color of each data point is the measured reflectivity and the underlying color filling is associated to the reflectivity fit. The hydrogen density is estimated using the ab-initio EoS of Ref. 42 which is in good agreement with experiment[23]. The density-temperaturepaths of the two H-He hugoniot curves measured here, for 11 mol% He at 4 GPa pre-compression and for 33 mol% He at 2 GPa pre-compression, are plotted as full and dashed black lines respectively.

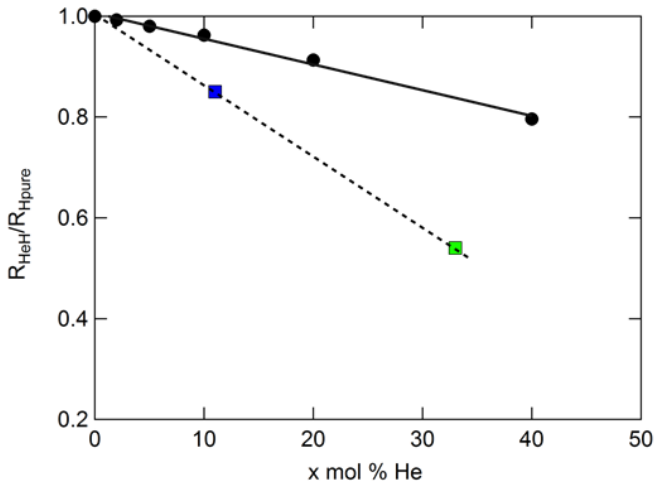

Extended Data Fig. 3: Saturated value of reflectivity along the Hugoniot of the pre-compressed H-He mixture versus He concentration. The saturation of reflectivity relative to that of pure hydrogen is plotted versus the He concentration. The squares indicate the experimental values, as shown by the horizontal dashed-lines in Fig. 3, blue and green for the 11 and 33 mol% He mixtures, respectively. Black dots are calculations of ref. 25.

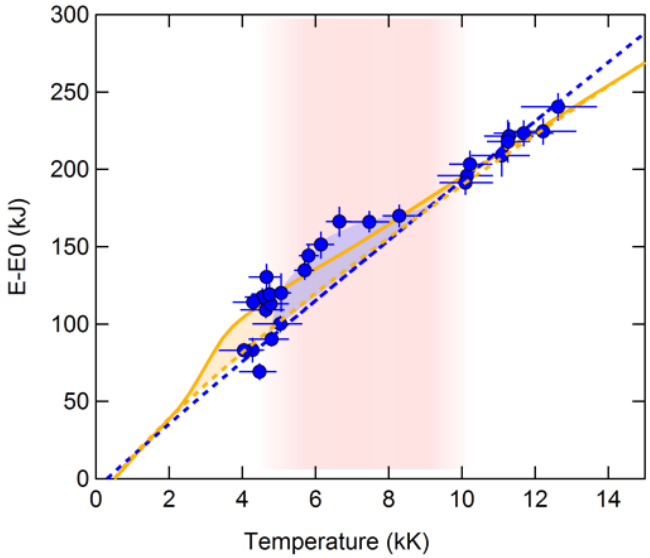

Extended Data Fig.4: Energy versus temperature along the Hugoniot for a near protosolar H-He mixture pre-compressed to 4 GPa. Blue dots are experimental data points for the 11 mol% He mixture and the orange full line the calculated Hugoniot for a 8 mol% He mixture[24]. A bump deviation from a smooth sublinear evolution, as dashed lines, should be associated to the molecular dissociation and conducting transition.

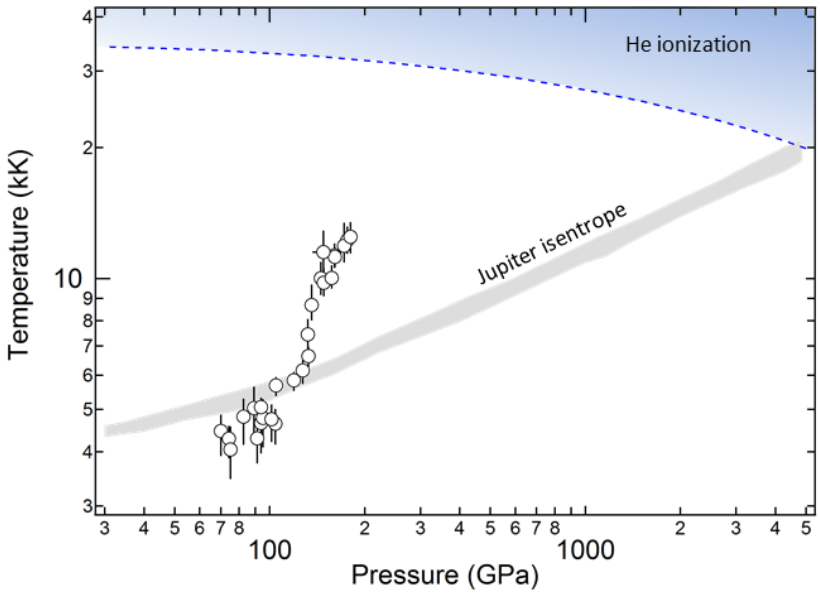

Exttended Data Fig.5: Boundary for Helium ionization. The solid blue zone indicates where a few % ionization of He start to appear. That is based on the experimental He reflectivity[19] subsequently analyzed by Soubiran[28] in the framework of an intrinsic semiconductor model with a gap energy depending on density and temperature. The blue dashed-line is drawn using the He gap model[28] and the REoS table to estimate the He density[34]. The intrinsic ionization fraction of He depends exponentially on E_g/K_BT. The level of He ionization sufficient to perturb the H-He miscibility properties is taken when temperature is getting greater than $E_g/3K_B$, so entering the blue domain. The present Hugoniot data points, as circles, are far from this boundary. The Jupiter's isentrope is crossing the He ionization domain only at its central maximum pressure. He ionization should not take place inside Jupiter.

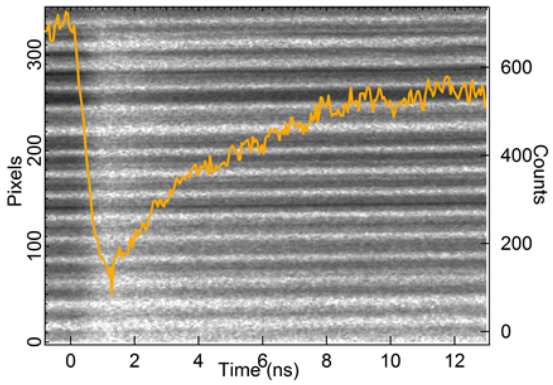

Extended data Fig.6. Transient opacification of the diamond window. VISAR Image taken through a blanking diamond window. The average intensity over several fringes is plotted on top of the image, as the orange curve. The recovery of the transmission of the diamond anvil is observed. It can be fitted with an exponential evolving transmission with a time scale of 3.7 ns.

Extended Data Table 1: 11 mole % He Hugoniot data

Extended Data Table 2: 33 mole % He Hugoniot data

Extended Data Table 3: 6 GPa D2 Hugoniot data